Heliyon 9 (2023) e16069

Contents lists available at ScienceDirect

Heliyon

journal homepage: www.cell.com/heliyon

Research article

Influence of Al doping in zinc oxide electron transport layer for the degradation triple-cation-based organometal halide perovskite solar cells

Firoz Khan [a,*], Vakeel Ahmad [b], Thamraa Alshahrani [c,**], Awatef Salem Balobaid [d], Abdulaziz M. Alanazi [e]

[a] Interdisciplinary Research Center for Renewable Energy and Power Systems (IRC-REPS), King Fahd University of Petroleum & Minerals (KFUPM), Dhahran 31261, Saudi Arabia
[b] Centre of Excellence in Renewable Energy Education and Research, Faculty of Science, University of Lucknow (New Campus), Lucknow, U.P. 226021, India
[c] Department of Physics, College of Science, Princess Nourah bint Abdulrahman University, Riyadh, 11671, Saudi Arabia
[d] Department of Computer Science, Computer Science and Information Technology College, Jazan University, Jazan 45142, Saudi Arabia
[e] Department of Chemistry, Faculty of Science, Islamic University of Madinah, Madinah 42351, Saudi Arabia

ARTICLE INFO

Keywords:
Triple cation perovskite
Perovskite solar cells
Degradation of solar cells under humidity
Temperature effect
Photovoltaic cell parameters

ABSTRACT

Various strategies have been adapted to fabricate stable organic-inorganic hybrid perovskite (PVT) solar cells (PSCs). The triple-cation ($CH_3NH_3^+$ (MA^+), $CH_3(NH_2)^{2+}$ (FA^+), and Cs^+) along with dual-anion (I^- and Br^-)-based PVT (TC-PVT) layer offers better stability than single cation-based PVTs. The deprivation of the PVT absorber is also influenced by the interface of the absorber with the charge transport layer (electron transport layer (ETL) and hole transport layer (HTL)). Here, the degradation of the TC-PVT coated on Al-doped zinc oxide (AZO) as well as FTO/AZO/TC-PVT/HTL structured PSC was examined for various Al to Zn molar ratio ($R_{Al/Zn}$) of AZO. The PL decay study of FTO/AZO/TC-PVT revealed that the lowest degradation in the power (35.38%) was observed for the AZO with $R_{Al/Zn}$ of 5%. Furthermore, the PV cell parameters of the PSCs were analytically determined to explore the losses in the PSCs during degradation. The shunt resistance reduction was maximum (50.32%) for $R_{Al/Zn}$ = 10%, whereas, minimum shunt loss (7.33%) for $R_{Al/Zn}$ of 2%. The highest loss due to series resistance was observed for $R_{Al/Zn}$ of 0%. The changes in diode ideality factor (n) and reverse saturation current density (J_0) were the smallest for $R_{Al/Zn}$of 10%.

1. Introduction

Recently, organometal halide perovskite (PVT) materials have been paid more attention as solar radiation absorbers [1–3]. The power conversion efficiency (η) of PVT-based solar cells (PSCs) has risen steeply from 3.8% to more than 25.7% in just a few years [4]. The PVT active layer can be synthesized via a solution process [2], and it offers a tunable optical bandgap [5]. Moreover, PVT exhibits high absorption and exceptional carrier lifetimes [6,7].

* Corresponding author.
** Corresponding author.
E-mail addresses: firoz.khan@kfupm.edu.sa (F. Khan), thmalshahrani@pnu.edu.sa (T. Alshahrani).

https://doi.org/10.1016/j.heliyon.2023.e16069
Received 10 February 2023; Received in revised form 30 April 2023; Accepted 4 May 2023
Available online 6 May 2023

Thus, PSCs are attracting more attention from the photovoltaic (PV) community [8–10]. However, the stability issue limits their practical application [11]. The presence of weak Pb-X bonds in PVT is the key factor for the degradation of the PVT layer under UV radiation, hot, and humid environments (X stands for Cl, Br, or I) [12,13]. The degradation of the PSCs can be alleviated via the formation of the high-quality PVT layer [14] as well as the selection of the charge transport layers. Generally, n-type material is used as an electron transport layer (ETL), however, p-type material is used as a hole transport layer (HTL) [15,16]. The rate of degradation of the PVT layers is slow at a temperature below 85 °C, nevertheless, a quick degradation was observed at elevated temperatures [17,18]. It was observed that the $CH_3NH_3PbI_3$ perovskite layer can easily decompose into PbI_2 and CH_3NH_3I in open air or moisture [19,20]. Moreover, the $CH_3(NH_2)_2PbI_3$ perovskite layer exhibits two phases; the first (α)-phase is promising for solar cell application [21]. However, the second (δ)-phase is unresponsive to light, thus, unfortunate for PSCs [21]. Besides, the α-phase can easily convert into the δ-phase in presence of air or moisture [22]. However, triple-cation ($CH_3NH_3^+$ (MA^+), $CH_3(NH_2)_2^+$ (FA^+), Cs^+) along with dual-anion (I^- and Br^-)-based PVT (TC-PVT, $Cs_{0.05}(FA_{0.77}MA_{0.17})Pb(I_{2.53}Br_{0.47})$) layer offers better stability than single cation-based PVTs [23,24]. The formation of Cs-X ionic bonding is also improving the stability of the TC-PVT absorber.

It was observed that inorganic ETLs provide more stable PSCs than organic ETLs. Among the inorganic ETLs, ZnO has admirable electron mobility and is easy to coat, which offers superior and cost-effective PSCs [25]. Nevertheless, several charge trap centers are created at the interface between ZnO and PVT, which lessens the η of the PSCs [25]. The performance and stability of the ZnO-based PSCs can be improved by replacing the ZnO with Al-doped ZnO (AZO) [26]. The dependency of the performance of AZO-based PSC on Al doping was already investigated [27]. The degradation of the PSCs is also important to be investigated for the deployment of the technology [28]. In this regard, the performance parameter degradation was investigated in our previous study [27]. The losses that occurred during the degradation can be examined via analysis of the PV cell parameters (photogenerated current density (J_{ph}), shunt resistance (R_{sh}), series resistance (R_s), diode ideality factor (n), and reverse saturation current density (J_0)). Because the performance of the PV devices is directed by the PV cell parameters [29]. Thus, the investigation of the PV cell parameters is vital to analyze the losses occurring during the degradation of the PSCs.

In this work, the degradation of $Cs_{0.05}(FA_{0.77}MA_{0.17})Pb(I_{2.53}Br_{0.47})$ triple-cation and double-anion TC-PVT is on AZO layers (various Al/Zn molar ratio ($R_{Al/Zn}$)) using time-resolved photoluminescence decay analysis. Furthermore, the PV cell parameters of the AZO ETL-based PSCs were analytically predicted using the illuminated current density-voltage (J-V) characteristics. By analysis of the PV cell parameter, the origin of the losses was examined.

2. Theoretical

The PV cell parameters were predicted analytically [30] using Eqs. (1)–(5). This technique uses the inverse of slopes 1/(dJ/dV) of an illuminated current density-voltage (J-V) characteristic at open (R_{oc}) and short (R_{sc}) circuit conditions. For the determination of the PV cell parameters, the voltage and current density at maximum power point along with thermal voltage ($V_T = kT/q$) are also needed. Where, k = Boltzmann's constant, T = temperature of the PSCs, and q = charge of the electron [29].

$$R_{sh} = R_{sc} \tag{1}$$

$$n = \frac{(V_m + R_{oc}J_m - V_{oc})}{V_T\left\{ln\left(J_{sc} - \frac{V_m}{R_{sc}} - J_m\right) - ln\left(J_{sc} - \frac{V_{oc}}{R_{sh}}\right) + \frac{J_m}{J_{sc} - \left(V_{oc}/R_{sc}\right)}\right\}} \tag{2}$$

$$J_0 = \left(J_{sc} - \frac{V_{oc}}{R_{sh}}\right)e^{-\left(\frac{V_{oc}}{nV_T}\right)} \tag{3}$$

$$R_s = R_{oc} - \frac{nV_T}{J_0}e^{-\left(\frac{V_{oc}}{nV_T}\right)} \tag{4}$$

$$J_{ph} = J_{sc}\left(1 + \frac{R_s}{R_{sh}}\right) + J_0\left(e^{\left(\frac{J_{sc}R_s}{nV_T}\right)} - 1\right) \tag{5}$$

The PV cell parameters can be predicted as follows:

(i) R_{sh} is predicted using Eq. (1)
(ii) The value of n is predicted using Eq. (2)
(iii) J_0 is predicted using Eq. (3)
(iv) R_s is predicted Eq. (4)
(v) J_{ph} is predicted using Eq. (5)

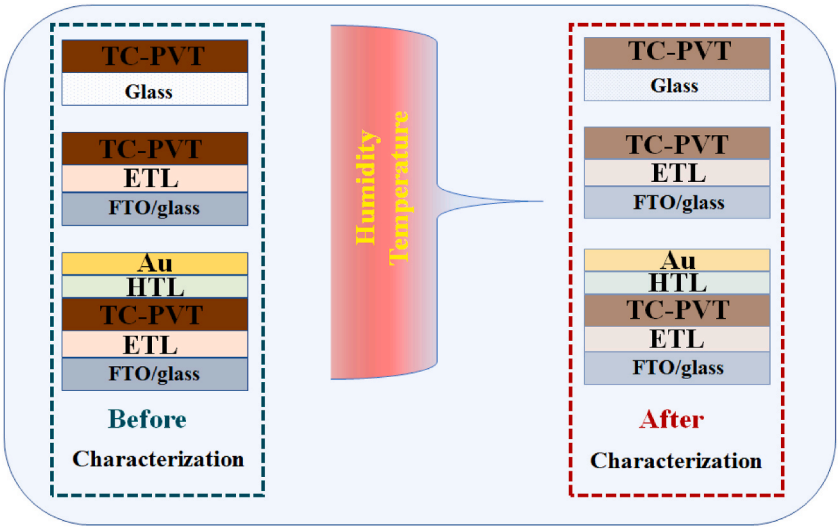

Fig. 1. Schematic of the methodology adopted for the degradation study.

3. Materials and methods

3.1. Chemicals

Zinc acetate dehydrate (99.999%), aluminum nitrate nonahydrate (99.99%), methanol (anhydrous, 99.8%), potassium hydroxide (KOH, ≥85%), formamidinium iodide (FAI, anhydrous, ≥99%), methylammonium iodide (MAI, anhydrous, ≥99%), lead iodide (PbI_2, 99.999%), lead iodide ($PbBr_2$, 99.999%), dimethyl sulfoxide (DMSO, anhydrous, 99.9%), and N,N-dimethylformamide (DMF, anhydrous, 99.8%) were purchased from Sigma-Aldrich.

3.2. Material synthesis

The AZO nanoparticles (AZO NPs) were coated for the ETL formation. The zinc acetate dihydrate and aluminum nitrate nonahydrate precursors were used as Zn and Al sources, respectively. The detailed synthesis process is reported elsewhere [31]. In brief, the zinc acetate dihydrate was dissolved in methanol (107.2 mol/L) including aluminum nitrate nonahydrate with an Al to Zn molar ratio ($R_{Al/Zn}$) of 1 to 10%. The chemical reaction was carried out at 65 °C by adding KOH (dissolved in methanol) during the stirring. After stirring for 4 h, the resulting solution was kept to precipitate AZO NPs. The NPs were collected via filtration followed by washing in methanol. Finally, the AZO NPs were annealed at 500 °C for 1 h in air. Hereafter, the AZO NPs with $R_{Al/Zn} = 0\%$, 1%, 2%, 5%, and 10% will be mentioned as AZO0, AZO1, AZO2, AZO5, and AZO10, respectively. For simplicity, undoped ZnO was referred to as AZO0. The AZO NPs were depressed in 1-butanol to get an AZO solution of concentration 10 mg/ml.

To synthesize the perovskite layer, FAI, MAI, PbI_2, and $PbBr_2$ were dissolved in the mixed solvent of DMSO and DMF in 1:4 (v/v). The concentrations of the FAI, MAI, PbI_2, and $PbBr_2$ were 1.0, 0.2, 1.1, and 0.2 M, respectively. A separate solution was prepared by dissolving 5% (wt./vol.) in DMSO, which was added to the first solution. The details synthesis process can be found elsewhere [23,24]. However, the HTL was synthesized as per our previous report [31].

3.3. Material characterization

The crystallinity of the samples was studied using X-ray diffraction (XRD; Empyrean, PanAnalytical HR-XRD system). Atomic force microscopy (AFM) (M/s Park systems, XE-150) was used to examine the surface roughness. The morphology of the TC-PVT layer was elucidated using field-emission scanning electron microscopy (FESEM, Model: S-4800) was employed. The absorbance spectra were acquired using PerkinElmer UV–Vis–NIR (Model: Lamda 750). Hamamatsu spectrofluorometer (Model: C10627) was used to acquire the time-resolved photoluminescence (TRPL) spectra of the TC-PVT layer.

3.4. PSC fabrication

Fluorine-doped tin oxide (FTO) glass was washed away with detergent. After drying, the FTO was cleaned in isopropanol and ethanol via sonicated. Then boiled piranha solution was used for further cleaning followed by drying in N_2. The samples were Ozone treated before ZnO barrier layer deposition via an atomic layer deposition (ALD) process [32]. AZO ETL layer was applied via spin coating of the AZO solution to prepare ETL at a spin speed of 3000 rpm for 60 s. The TC-PVT layer formed a two-step spin-coating process (1000 rpm for 10 s + 4000 rpm for 20 s). Then the perovskite layer was annealed at 100 °C for 30 min under an N_2 atmosphere.

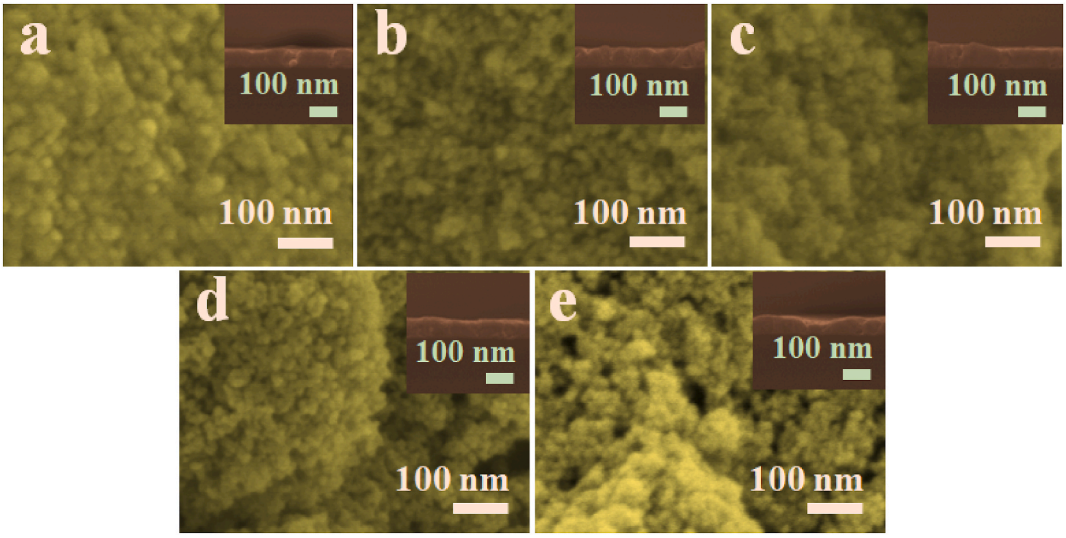

Fig. 2. Field emission scanning electron microscopy (FESEM) images of (a) AZO0, (b) AZO1, (c) AZO2, (d) AZO5, and (e) AZO10 nanoparticles. In the inset, corresponding cross-sectional FESEM images.

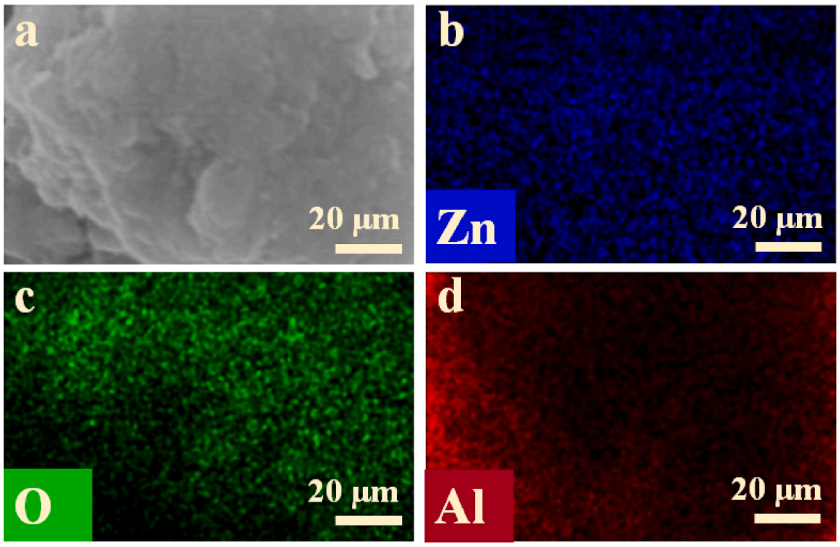

Fig. 3. The energy dispersive X-ray spectroscopy (EDS) of AZO10.

The HTL layer was deposited at 4000 rpm for 30 s. The TC-PVT and HTL layers were coated in an Ar-filled glove box. The contact was made via Au (80 nm) deposition using electron beam evaporation.

3.5. PSC characterization

The active area of the cells used for J-V characteristics was ~0.05 cm^2. The J-V characterization was carried out using a source-meter (Keithley, Model: 2400) under simulated illumination (AM1.5G) of intensity 100 mW/cm^2. The simulated illumination was obtained from a solar simulator system (M/s New-port, 91192). The illumination intensity was calibrated using a silicon solar cell (reference cell) obtained from PV Measurement Incorporation, USA.

3.6. Degradation study

The degradation study was carried out for the TC-PVT layer coated on the bare glass as well as on Glass/ETL. The perovskite layer along with PSCs was retained in the open atmosphere for 7 days. The samples were characterized via visualization, XRD, FESEM, PL

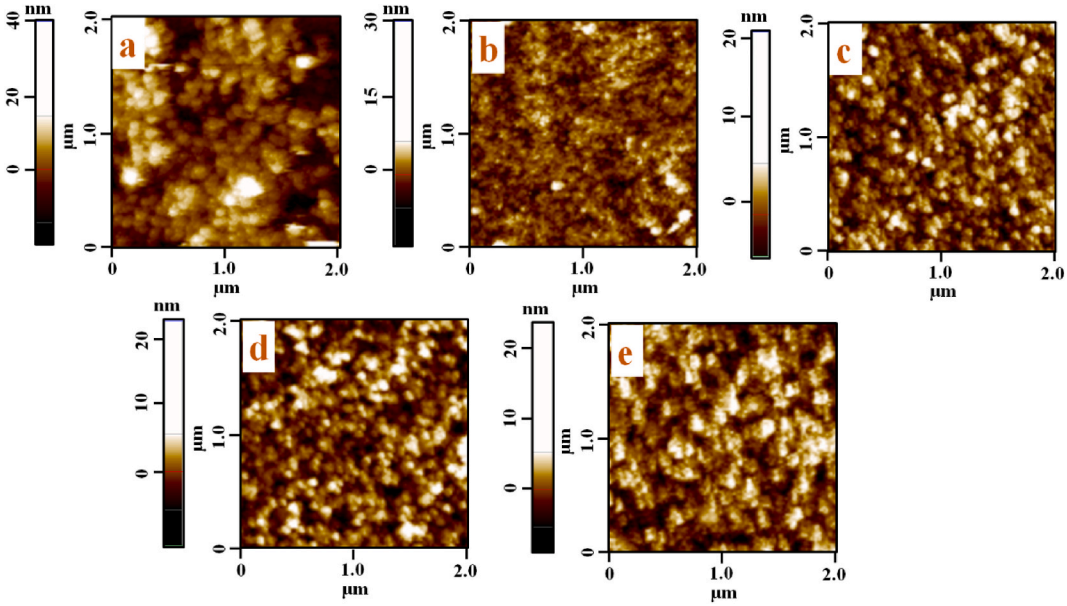

Fig. 4. AFM images of AZO ETL for Al/Zn molar ratio of (a) 0%, (b) 1%, (c) 2%, (d) 5%, and (e) 10%, coated on the glass surface.

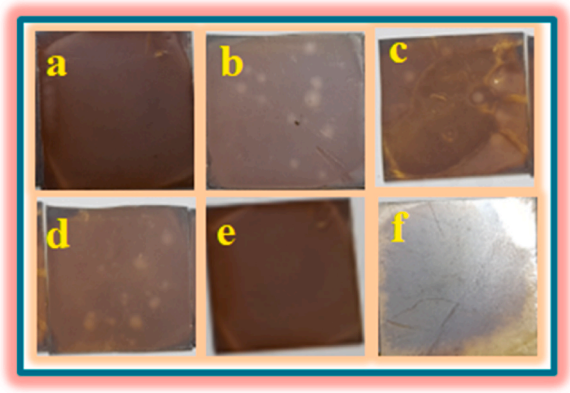

Fig. 5. Optical images of (a) freshly coated TC-PVT layer, degraded TC-PVT layer on glass/AZO for Al contents of (b) 0%, (c) 1%, (d) 2%, (e) 5%, and (f) 10%.

decay, and J-V measurement to examine the degradation of the perovskite layers and cells. The performance and PV cell parameters were analyzed to examine the degradation in the cells. The schematic for the degradation study is illustrated in Fig. 1.

4. Results and discussion

4.1. Morphological properties of AZO

The morphological studies of the AZO NPs were carried out before AZO layer formation. Fig. 2 displays the FESEM images of the agglomerated AZO NPs. Furthermore, the AZO layers are coated on the glass surface to study the root mean square (RMS) surface roughness of the AZO ETLs. The energy dispersive X-ray spectroscopy (EDS) analysis was carried out for the elemental analysis. The EDS mapping of AZO10 confirms the doping of Al in ZnO. Also, the elements are uniformly distributed over the surface (Fig. 3a–d). The elemental composition was also determined by an X-Ray fluorescence (XRF) spectrometer. The values of $R_{Al/Zn}$ obtained for AZO1, AZO2, AZO5, and AZO1O are 0.98, 1.94, 4.87, and 9.57%, respectively. The AFM images of the AZO ETLs are shown in Fig. 4. The obtained RMS surface roughness values are 6.50, 4.68, 4.12, 3.18, and 4.63 nm for the ETL of AZO0, AZO1, AZO2, AZO5, and AZO10, respectively.

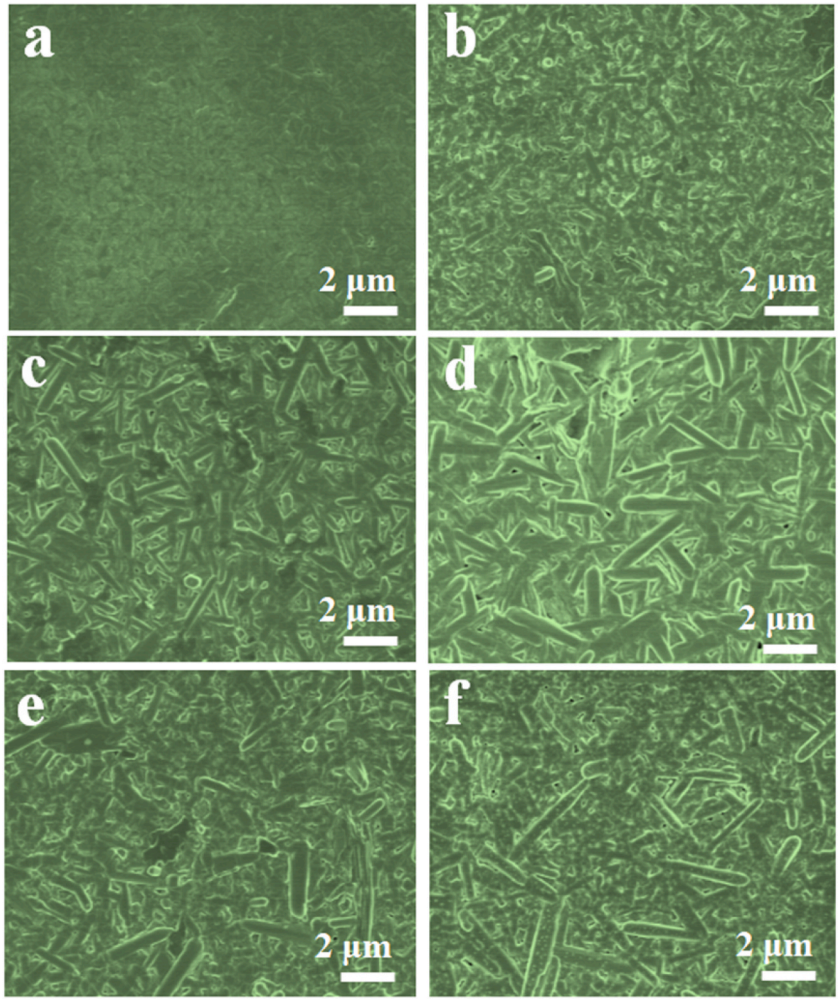

Fig. 6. Field emission scanning electron microscopy images of (a) freshly coated TC-PVT layer, degraded TC-PVT layer AZO ETL for Al/Zn molar ratio of (b) 0%, (c) 1%, (d) 2%, (e) 5%, and (f) 10%.

4.2. Visual inspection of TC-PVT layers

For the visual inspection of the degraded TC-PVT layer under varying humidity, the optical images of the TC-PVT layers deposited onto bare glass and glass/AZO are shown in Fig. 5. The fresh TC-PVT coated layer on bare glass is considered as a reference sample (Fig. 5a). It can be seen that the freshly coated sample has a dark brown color. Fig. 5(b–f) shows the optical images of the degraded TC-PVT coated onto the AZO layers of various $R_{Al/Zn}$. It seems that the color TC-PVT layer for $R_{Al/Zn} = 0\%$ (Fig. 5b) and $R_{Al/Zn} = 10\%$ (Fig. 5f) was greatly affected, which confirmed that an immense degradation has occurred in the TC-PVT layers coated onto glass/AZO0 and glass/AZO10. However, the colors of the TC-PVT on the glass/AZO1 (Fig. 5c) and glass/AZO2 (Fig. 5d) are slightly changed. Thus, it revealed a minor degradation in the TC-PVT layers for the Al contents of 1 and 2%. The least color change of TC-PVT is obtained for $R_{Al/Zn} = 5\%$, which indicates the lowermost degradation of the TC-PVT layer for $R_{Al/Zn} = 5\%$ (Fig. 5e).

4.3. Morphology of the TC-PVT

The surface morphologies of the perovskite layer coated on bare glass, and Glass/ETL are illustrated in Fig. 6. The nanorod-like shape is created in the samples; however, the size varies on different substrates. The observed length of the nanorods is 500 nm and 2 μm for the TC-PVT layers deposited on bare glass and AZO0, respectively. The length of the nanorod-like structures in other samples varies from 2 to 6 μm. The large grain size was observed for the glass/AZO1, glass/AZO2, glass/AZO5, and glass/AZO10, which revealed that the grain size of the TC-PVT layer depends on the Al doping of the AZO ETL. Thus, the degradation can vary with the Al doping concentration. It was observed that few pinholes are created the after degradation of the TC-PVT layers coated on glass/AZO0 and glass/AZO10 substrates (Fig. 6b and f). The degradation was slightly reduced for the Al doping concentration of 1 and 2% (Fig. 6c and d). However, the least degradation was observed for the Al doping concentration of 5% (Fig. 6e). The cross-sectional

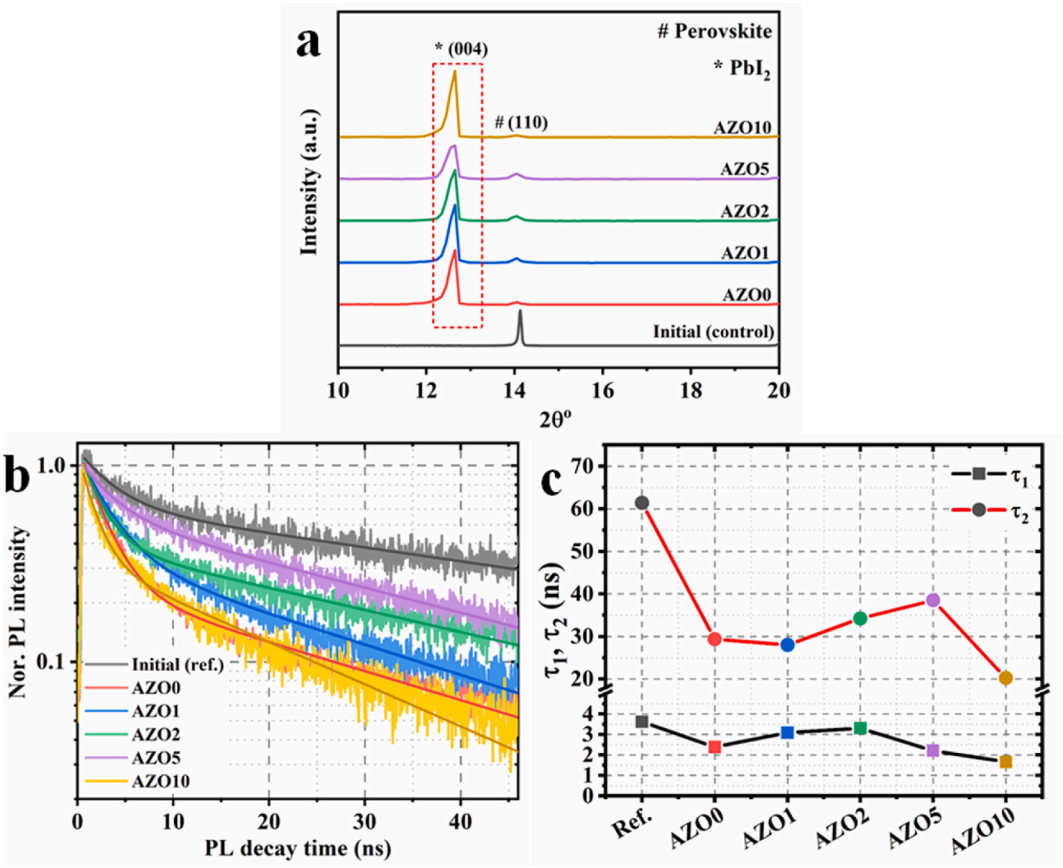

Fig. 7. XRD spectra of (a) freshly coated TC-PVT layer, degraded TC-PVT layer, (b) PL decay curves, and (c) PL decay lifetime of freshly coated TC-PVT layer and degraded TC-PVT layer on glass/AZO.

Table 1
The fitting parameters of the PL decay curves using a bi-exponential model.

Sample	A_1	τ_1 (ns)	A_2	τ_2 (ns)
Ref.	0.57	3.62	0.62	61.39
AZO0	1.06	2.39	0.24	29.37
AZO1	0.81	3.09	0.35	28.01
AZO2	0.52	3.31	0.57	34.25
AZO5	0.84	2.21	0.4	38.51
AZO10	0.85	1.66	0.33	20.21

Thus, a lower degradation is observed in the glass/AZO5/TC-PVT sample. However, for the TC-PVT on AZO10, the lowest value of τ_2 is obtained, which indicates that an uppermost degradation occurred in the TC-PVT layer onto AZO10.

FESEM images are shown in the inset of Fig. 6a–e. The observed thicknesses of the AZO layers (~100 nm) are nearly the same in all the samples.

4.4. Structural property of TC-PVT

It was observed in our previous study that the TC-PVT layer offered XRD peaks at 14.14°, 20.04°, 24.62°, 28.43°, and 31.92°, which are allied to (110), (200), (202), (220), and (310) diffraction planes of PVT, respectively (Fig. 7a) [33]. The peak present at $2\theta = 14.14^{o}$ revealed the formation of the tetragonal structure [34]. An additional peak at $2\theta = 12.65^{o}$ relating to the (004) plane of PbI_2 arose in all the degraded samples, which was not seen in the freshly deposited TC-PVT layer. The TC-PVT layer coated on AZO10 showed the highest degradation, while the lowest deprivation was observed for the TC-PVT layer deposited on AZO5. Thus, AZO5 ETL can be beneficial for the fabrication of stable PSCs.

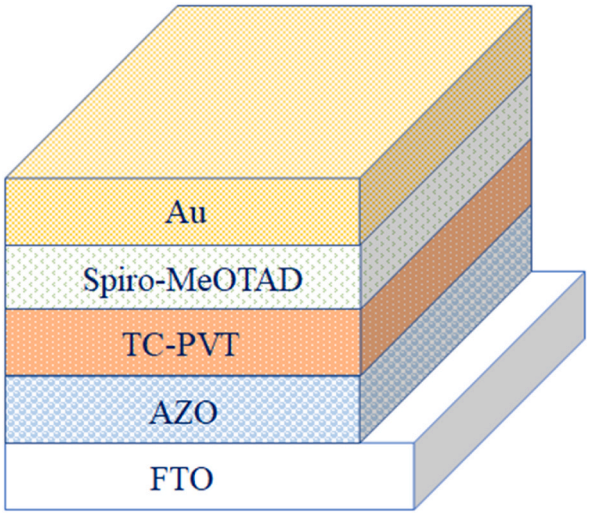

Fig. 8. Schematic of the structure of the triple-cation-based perovskite solar cell.

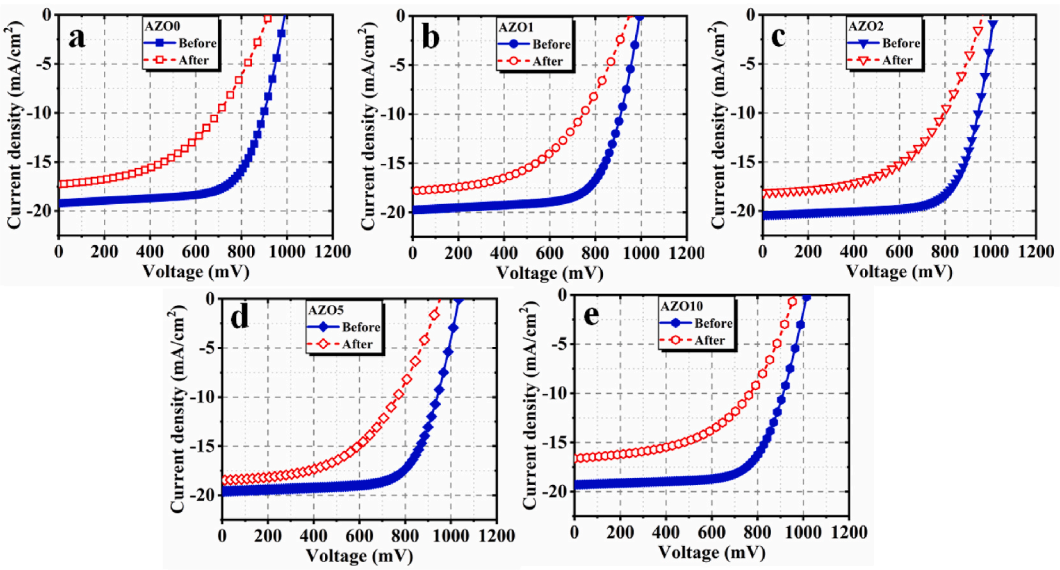

Fig. 9. Comparison of J-V characteristics of the perovskite solar cells before and after degradation for used ETL (a) AZO0, (b) AZO1, (c) AZO2, (d) AZO5, and (e) AZO10.

4.5. Photoluminescence properties

The TRPL spectra of the TC-PVT layers deposited on glass and ETL are shown in Fig. 7b. The decay in the TRPL spectra exhibited a similar inclination as in the PL [27]. The bi-exponential decay model is employed to fit the experimental data. Thus, the PL decay lifetimes were calculated using Eq. (6) [35].

$$I(t) = B_1 \exp\left(\frac{t}{\tau_1}\right) + B_2 \exp\left(\frac{t}{\tau_2}\right) \tag{6}$$

where, $I(t)$ = PL intensity, B_1 and B_2 = proportion constants, τ_1 = faster decay constant, and τ_2 = slower decay constant.

The value of τ_1 is accompanied by the diffusion of photogenerated excitons into defects, however, τ_2 is related to exciton lifetime [36]. The fitting parameters are tabulated in Table 1. The value of τ_2 can be used for degradation analysis. The TC-PVT layers are deposited on glass/AZO (no conducting layer between glass and AZO), so there is no charge extraction. In this case, the reduction in the value of τ_2 is indicative of the degradation. The variation of the τ_1 and τ_2 is illustrated in Fig. 7c. The TC-PVT layer coated on the glass/AZO exhibited a slightly lower τ_1 than that deposited on the bare glass. The value of τ_2 is reduced to 29.37 ns after degradation of

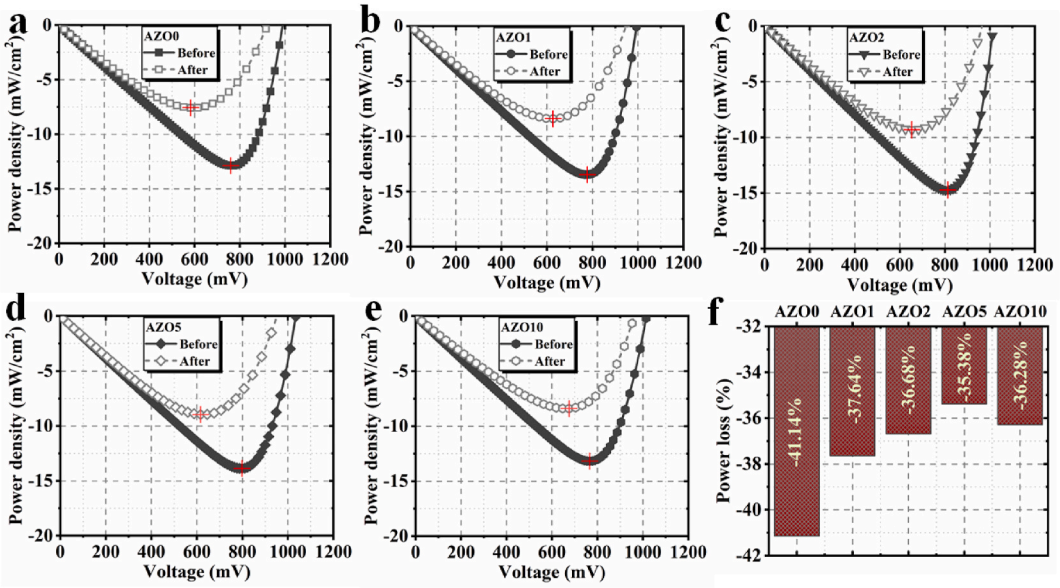

Fig. 10. Comparison of P–V characteristics of the perovskite solar cells before and after degradation for used ETL (a) AZO0, (b) AZO1, (c) AZO2, (d) AZO5, (e) AZO10, and (f) power losses during degradation of PSCs.

Table 2
Theoretically predicted PV parameters before degradation.

ETL	J_{ph} (A/cm^2)	R_{sh} (Ωcm^2)	R_s (Ωcm^2)	n	J_0 (A/cm^2)
AZO0	0.01931	806.45	5.20	2.1338	2.5×10^{-10}
AZO1	0.01988	819.67	5.15	1.9473	4.45×10^{-11}
AZO2	0.02044	990.10	4.33	1.8328	8.67×10^{-12}
AZO5	0.01973	1075.27	6.97	1.4739	4.28×10^{-14}
AZO10	0.01939	1265.83	6.50	2.4240	1.12×10^{-9}

Table 3
Theoretically predicted PV parameters after degradation.

ETL	J_{ph} (A/cm^2)	R_{sh} (Ωcm^2)	R_s (Ωcm^2)	n	J_0 (A/cm^2)
AZO0	0.01757	588.24	9.79	5.1820	1.57×10^{-5}
AZO1	0.01802	735.29	7.78	5.4172	1.86×10^{-5}
AZO2	0.01828	917.43	7.52	4.7253	6.01×10^{-6}
AZO5	0.01866	990.11	10.29	4.3395	3.43×10^{-6}
AZO10	0.01682	558.66	6.02	5.0785	9.56×10^{-6}

the TC-PVT layer coated on AZO of $R_{Al/Zn} = 0\%$, however, the initial value of τ_2 is 61.39 ns. This result revealed that a large degradation occurred for the TC-PVT coated onto glass/AZO0. The value of τ_2 is slightly reduced to 28.01 ns for $R_{Al/Zn} = 1\%$. With a further rise in $R_{Al/Zn}$, the value of τ_2 is increased. It attained the value of 34.25 and 38.51 ns for the TC-PVT layer on coated AZO2 and AZO5, respectively.

4.6. PV cell parameter analysis

Fig. 8 represents the schematic of the n-i-p structured PSC used for this study. The illuminated J-V curves obtained before and after degradation is elucidated in Fig. 9a–e. These J-V curves were used to determine the PV cell parameters. The power density-voltage curves are illustrated in Fig. 10a–e. The maximum power point is denoted by the "+" symbol. The overall power loss is represented in Fig. 10f. The theoretically predicted PV cell parameter values before and after degradation are provided in Tables 2 and 3, respectively. The reliance on the PV cell parameters is elucidated in Fig. 11a–e. The deviations in the PV cell parameters are shown in Fig. 12a–e. The trend of change in J_{ph} is the same as in J_{sc}. After degradation, the losses in the J_{sc} values are found to be 9.04%, 9.39%, 10.62%, 5.35%, and 13.02% for the PSCs of AZO0, AZO1, AZO2, AZO5, and AZO10 ETLs, respectively. This confirms that the maximum destruction in J_{sc} is found for AZO10 ETL-based PSC. The values of R_{sh} are reduced by 27.05%, 10.29%, 7.33%, 7.92%, and 50.32% for $R_{Al/Zn} = 0\%$, 1%, 2%, 5%, and 10%, respectively. The lowest change in R_{sh} is obtained for AZO2, while the drop in R_{sh} value

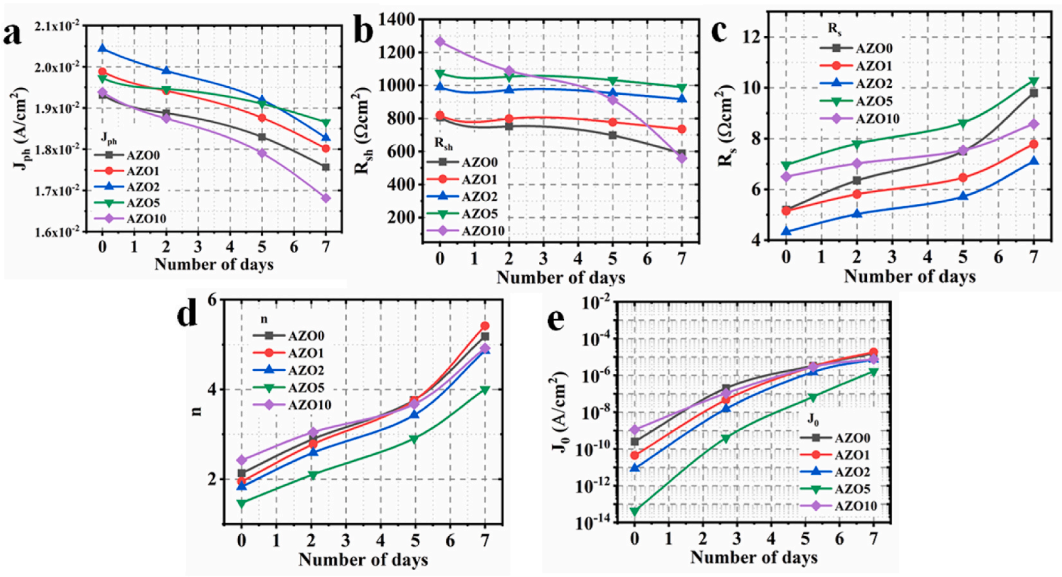

Fig. 11. The variation of PV cell parameters with degradation time.

is the highest for AZO10 ETL-based PSC. The shunting is arisen due to leakage current caused by the formation of pinholes or short-circuiting at the edge of the PSCs. Usually, the R_{sh} is interrelated to the localized defect regions containing many trap centers. For an ideal PSC, the shunt resistance should be infinite. However, other remaining PV cell parameters are increased after degradation. The related enhancement in the R_s values for AZO0, AZO1, AZO2, AZO5, and AZO10 are found to be 88.36%, 51.05%, 64.06%, 47.66%, 31.92%, respectively. The largest increase of R_s is obtained for AZO0, while the lowest change is found for AZO10. The rise in series resistance is due to an increase in the bulk resistances of the TC-PVT layer or interfaces (between PVT and charge-transporting layers, or between contacts and charge-transporting layers) during degradation of the PSCs. The n values are greatly increased for the degraded PSCs.

The relative changes in the n values are 142.85%, 178.19%, 165.31%, 171.73%, and 102.94% for AZO0, AZO1, AZO2, AZO5, and AZO10 ETL-based PSCs, respectively. After the degradation of the PSCs, the changes in the J_0 are found to be too large. The lowest rise in the J_0 is obtained for AZO10 (~679428%). The values of n and J_0 are indicative of the recombination. Due to an increase in the recombination, the value of J_0 is enhanced. The smallest increase in the J_0 for AZO10 ETL-based PSC indicates lower recombination in the TC-PVT layer and at the interfaces between TC-PVT and the charge-transporting layers.

5. Conclusions

Triple-cation-based perovskite solar cells were fabricated using Al-doped zinc oxide as the electron transport layer. The Al/Zn molar ratio was varied from 0 to 10% to investigate the performance and degradation of AZO-based PSCs. The degradation of the perovskite layers coated on ETLs was investigated using PL decay. The utmost value of τ_2 for the degraded TC-PVT layer was 38.51 ns for $R_{Al/Zn} = 5\%$ ($\tau_2 = 61.39$ ns before degradation). This approves that the lowermost degradation was observed for the TC-PVT layer coated on AZO5. Additionally, the deviations in the PV cell parameters of the PSCs were calculated. The changes in J_{ph} and R_{sh} were extreme for AZO10. The lowest change in J_{ph} was obtained for AZO5, however, the smallest change in R_{sh} was found for AZO2. The change in R_s was highest for AZO0 ETL-based PSC. The minimum changes in n and J_0 were found for AZO10 ETL-based PSC.

Author contribution statement

Firoz Khan: Conceived and designed the experiments; Performed the experiments; Wrote the paper.
Vakeel Ahmad, Awatef Salem Balobaid, Abdulaziz M. Alanazi: Analyzed and interpreted the data; Wrote the paper.
Thamraa Alshahrani: Analyzed and interpreted the data; Contributed reagents, materials, analysis tools or data; Wrote the paper.

Data availability statement

Data will be made available on request.

Declaration of competing interest

The authors declare that they have no known competing financial interests or personal relationships that could have appeared to

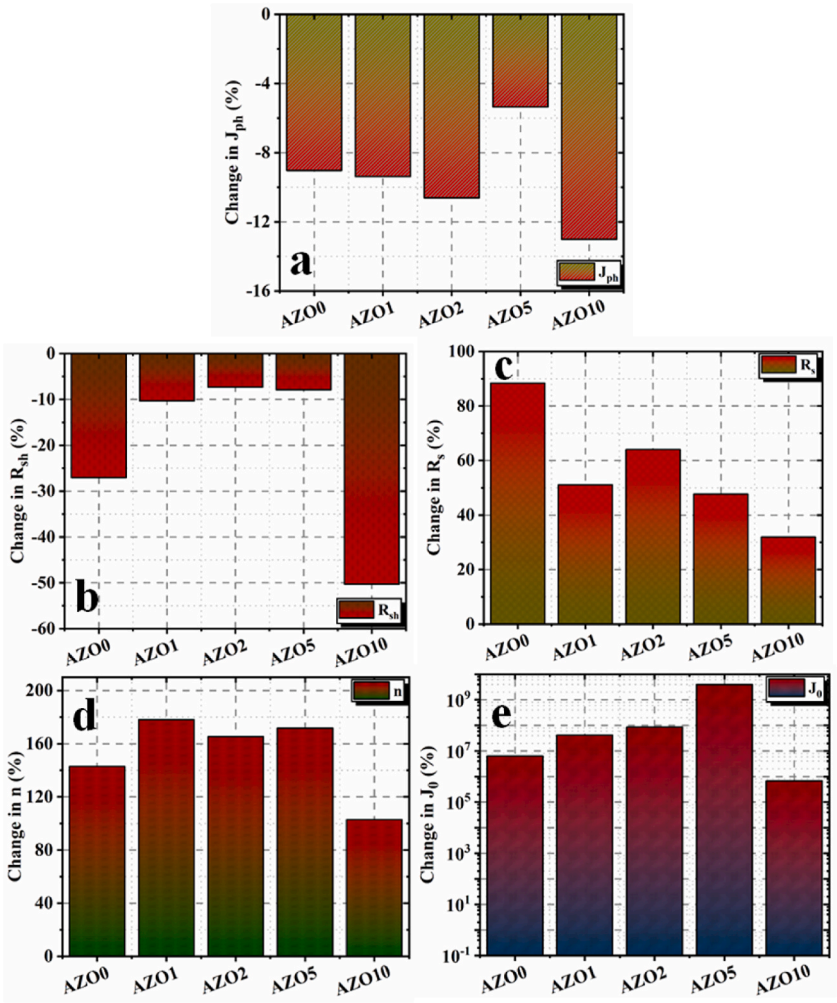

Fig. 12. The changes in PV cell parameters after degradation.

influence the work reported in this paper.

Acknowledgments

This research was funded by Princess Nourah bint Abdulrahman University, researchers supporting project number (PNURSP2023R1), Princess Nourah bint Abdulrahman University, Riyadh, Saudi Arabia. The authors also gratefully acknowledge King Fahd University of Petroleum & Minerals (KFUPM), Saudi Arabia.

References

[1] A. Kojima, K. Teshima, Y. Shirai, T. Miyasaka, Organometal halide perovskites as visible-light sensitizers for photovoltaic cells, J. Am. Chem. Soc. 131 (2009) 6050–6051.
[2] A. Chilvery, S. Das, P. Guggilla, C. Brantley, A. Sunda-Meya, A perspective on the recent progress in solution-processed methods for highly efficient perovskite solar cells, Sci. Technol. Adv. Mater. 17 (2016) 650–658.
[3] P. Mahajan, R. Datt, W. Chung Tsoi, V. Gupta, A. Tomar, S. Arya, Recent progress, fabrication challenges and stability issues of lead-free tin-based perovskite thin films in the field of photovoltaics, Coord. Chem. Rev. 429 (2021), 213633.
[4] S.S. Hegedus, E. Fagen, Midgap states in a-Si: H and a-SiGe: H p-i-n solar cells and Schottky junctions by capacitance techniques, J. Appl. Phys. 71 (1992) 5941–5951.
[5] S. Gholipour, M. Saliba, Chapter 1 - bandgap tuning and compositional exchange for lead halide perovskite materials, in: M. Pazoki, A. Hagfeldt, T. Edvinsson (Eds.), Characterization Techniques for Perovskite Solar Cell Materials, Elsevier, 2020, pp. 1–22.
[6] S.D. Stranks, G.E. Eperon, G. Grancini, C. Menelaou, M.J.P. Alcocer, T. Leijtens, L.M. Herz, A. Petrozza, H.J. Snaith, Electron-hole diffusion lengths exceeding 1 micrometer in an organometal trihalide perovskite absorber, Science 342 (2013) 341–344.
[7] H. Zhou, Q. Chen, G. Li, S. Luo, T.-b. Song, H.-S. Duan, Z. Hong, J. You, Y. Liu, Y. Yang, Interface engineering of highly efficient perovskite solar cells, Science 345 (2014) 542–546.

[8] S.D. Stranks, G.E. Eperon, G. Grancini, C. Menelaou, M.J. Alcocer, T. Leijtens, L.M. Herz, A. Petrozza, H.J. Snaith, Electron-hole diffusion lengths exceeding 1 micrometer in an organometal trihalide perovskite absorber, Science 342 (2013) 341–344.

[9] L.M. Pazos-Outón, M. Szumilo, R. Lamboll, J.M. Richter, M. Crespo-Quesada, M. Abdi-Jalebi, H.J. Beeson, M. Vrućinić, M. Alsari, H.J. Snaith, B. Ehrler, R. H. Friend, F. Deschler, Photon recycling in lead iodide perovskite solar cells, Science 351 (2016) 1430–1433.

[10] J. Nishida, A.H. Alfaifi, T.P. Gray, S.E. Shaheen, M.B. Raschke, Heterogeneous cation–lattice interaction and dynamics in triple-cation perovskites revealed by infrared vibrational nanoscopy, ACS Energy Lett. 5 (2020) 1636–1643.

[11] S. Kundu, T.L. Kelly, In situ studies of the degradation mechanisms of perovskite solar cells, EcoMat 2 (2020), e12025.

[12] J. Khan, X. Zhang, J. Yuan, Y. Wang, G. Shi, R. Patterson, J. Shi, X. Ling, L. Hu, T. Wu, S. Dai, W. Ma, Tuning the surface-passivating ligand anchoring position enables phase robustness in CsPbI3 perovskite quantum dot solar cells, ACS Energy Lett. 5 (2020) 3322–3329.

[13] C.A. Rodríguez-Castañeda, P.M. Moreno-Romero, A.N. Corpus-Mendoza, G. Suárez-Campos, M. Miranda-Hernández, M. Sotelo-Lerma, H. Hu, Thermal evaporation–oxidation deposited aluminum oxide as an interfacial modifier to improve the performance and stability of zinc oxide-based planar perovskite solar cells, ACS Appl. Energy Mater. 3 (2020) 9618–9627.

[14] S.-M. Bang, S.S. Shin, N.J. Jeon, Y.Y. Kim, G. Kim, T.-Y. Yang, J. Seo, Defect-tolerant sodium-based dopant in charge transport layers for highly efficient and stable perovskite solar cells, ACS Energy Lett. 5 (2020) 1198–1205.

[15] H. Wei, S. Chen, J. Zhao, Z. Yu, J. Huang, Is formamidinium always more stable than methylammonium? Chem. Mater. 32 (2020) 2501–2507.

[16] P. Mahajan, A. Ahmed, R. Datt, V. Gupta, S. Arya, Chemically synthesized ZnO-WO3 nanoparticles as electron and hole transport layer in organic solar cells, ECS Trans. 107 (2022) 9199.

[17] Y. Cui, C. Chen, C. Li, L. Chen, S.S. Bista, X. Liu, Y. Li, R.A. Awni, Z. Song, Y. Yan, Correlating hysteresis and stability with organic cation composition in the two-step solution-processed perovskite solar cells, ACS Appl. Mater. Interfaces 12 (2020) 10588–10596.

[18] S. Yang, L. Wang, L. Gao, J. Cao, Q. Han, F. Yu, Y. Kamata, C. Zhang, M. Fan, G. Wei, T. Ma, Excellent moisture stability and efficiency of inverted all-inorganic CsPbIBr2 perovskite solar cells through molecule interface engineering, ACS Appl. Mater. Interfaces 12 (2020) 13931–13940.

[19] G.E. Eperon, S.D. Stranks, C. Menelaou, M.B. Johnston, L.M. Herz, H.J. Snaith, Formamidinium lead trihalide: a broadly tunable perovskite for efficient planar heterojunction solar cells, Energy Environ. Sci. 7 (2014) 982–988.

[20] Y. Han, S. Meyer, Y. Dkhissi, K. Weber, J.M. Pringle, U. Bach, L. Spiccia, Y.-B. Cheng, Degradation observations of encapsulated planar $CH_3NH_3PbI_3$ perovskite solar cells at high temperatures and humidity, J. Mater. Chem. 3 (2015) 8139–8147.

[21] T. Zhang, J. Wu, P. Zhang, W. Ahmad, Y. Wang, M. Alqahtani, H. Chen, C. Gao, Z.D. Chen, Z. Wang, S. Li, High speed and stable solution-processed triple cation perovskite photodetectors, Adv. Opt. Mater. 6 (2018), 1701341.

[22] C. Yi, J. Luo, S. Meloni, A. Boziki, N. Ashari-Astani, C. Grätzel, S.M. Zakeeruddin, U. Röthlisberger, M. Grätzel, Entropic stabilization of mixed A-cation ABX_3 metal halide perovskites for high performance perovskite solar cells, Energy Environ. Sci. 9 (2016) 656–662.

[23] M. Saliba, T. Matsui, J.-Y. Seo, K. Domanski, J.-P. Correa-Baena, M.K. Nazeeruddin, S.M. Zakeeruddin, W. Tress, A. Abate, A. Hagfeldt, Cesium-containing triple cation perovskite solar cells: improved stability, reproducibility and high efficiency, Energy Environ. Sci. 9 (2016) 1989–1997.

[24] D.Y. Park, H.R. Byun, H. Kim, B. Kim, M.S. Jeong, Enhanced stability of perovskite solar cells using organosilane-treated double polymer passivation layers, J. Kor. Phys. Soc. 73 (2018) 1787–1793.

[25] C. Roldán-Carmona, O. Malinkiewicz, A. Soriano, G. Mínguez Espallargas, A. Garcia, P. Reinecke, T. Kroyer, M.I. Dar, M.K. Nazeeruddin, H.J. Bolink, Flexible high efficiency perovskite solar cells, Energy Environ. Sci. 7 (2014) 994–997.

[26] X. Zhao, H. Shen, Y. Zhang, X. Li, X. Zhao, M. Tai, J. Li, J. Li, X. Li, H. Lin, Aluminum-doped zinc oxide as highly stable electron collection layer for perovskite solar cells, ACS Appl. Mater. Interfaces 8 (2016) 7826–7833.

[27] F. Khan, I. Fareed, M. Al-Rasheidi, N. Ahmad, A. Al-Ahmed, Z.M. Ahmed, M. Shariq, M.H. Zahir, Analysis of performance parameters during degradation of triple-cation-based organic–inorganic hybrid perovskite solar cells, Inorg. Chem. Commun. 135 (2022), 109094.

[28] T.A. Berhe, W.-N. Su, C.-H. Chen, C.-J. Pan, J.-H. Cheng, H.-M. Chen, M.-C. Tsai, L.-Y. Chen, A.A. Dubale, B.-J. Hwang, Organometal halide perovskite solar cells: degradation and stability, Energy Environ. Sci. 9 (2016) 323–356.

[29] F. Khan, S.-H. Baek, Y. Park, J.H. Kim, Extraction of diode parameters of silicon solar cells under high illumination conditions, Energy Convers. Manag. 76 (2013) 421–429.

[30] J. Phang, D. Chan, J. Phillips, Accurate analytical method for the extraction of solar cell model parameters, Electron. Lett. 20 (1984) 406–408.

[31] F. Khan, J. Hyun Kim, Enhanced charge-transportation properties of low-temperature processed Al-doped ZnO and its impact on PV cell parameters of organic-inorganic perovskite solar cells, Solid State Electron. 164 (2020), 107714.

[32] F. Khan, S.-H. Baek, J.H. Kim, Influence of oxygen vacancies on surface charge potential and transportation properties of Al-doped ZnO nanostructures produced via atomic layer deposition, J. Alloys Compd. 709 (2017) 819–828.

[33] P. Fan, D. Gu, G.-X. Liang, J.-T. Luo, J.-L. Chen, Z.-H. Zheng, D.-P. Zhang, High-performance perovskite $CH_3NH_3PbI_3$ thin films for solar cells prepared by single-source physical vapour deposition, Sci. Rep. 6 (2016), 29910.

[34] M.-H. Liu, Z.-J. Zhou, P.-P. Zhang, Q.-W. Tian, W.-H. Zhou, D.-X. Kou, S.-X. Wu, p-type Li, Cu-codoped NiOx hole-transporting layer for efficient planar perovskite solar cells, Opt Express 24 (2016) A1349–A1359.

[35] J.W. Jung, C.C. Chueh, A.K. Jen, A low-temperature, solution-processable, Cu-doped nickel oxide hole-transporting layer via the combustion method for high-performance thin-film perovskite solar cells, Adv. Mater. 27 (2015) 7874–7880.

[36] Z. Zhu, Y. Bai, T. Zhang, Z. Liu, X. Long, Z. Wei, Z. Wang, L. Zhang, J. Wang, F. Yan, High-performance hole-extraction layer of sol–gel-processed NiO nanocrystals for inverted planar perovskite solar cells, Angew. Chem. 126 (2014) 12779–12783.